Joint Pathology Center
Veterinary Pathology Services

WEDNESDAY SLIDE CONFERENCE 2024-2025

Conference #3 28 August 2024

CASE I:

Signalment:
2-3 month old, intact male guinea pigs (*Cavia porcellus*)

History:
These guinea pigs were from a control group on study at a contract research organization. A nodule was found in the heart during post-life processing. No clinical signs were noted prior to euthanasia.

Gross Pathology:
A poorly-demarcated, tan nodule expands the right or left ventricular free wall or the interventricular septum of the heart.

Microscopic Description:
The subendocardial muscle is regionally effaced by expansile, well-circumscribed foci of atypical cardiac myocytes that are arranged in bundles and streams. Atypical cardiac myocytes are plump polygonal and have distinct cell borders. These cells are markedly distended by clear vacuoles, pale eosinophilic granular material, and acidophilic bodies. Nuclei are round; have finely to coarsely stippled chromatin; frequently contain a single prominent nucleolus; and are occasionally surrounded by radiating, linear sarcoplasmic processes (spider cells). The surrounding cardiac myofibers are minimally compressed. Small numbers of mixed mononuclear cells multifocally infiltrate the normal cardiac muscle.

Figure 1-1. Heart, guinea pig. A longitudinal and a transverse section of the ventricles is submitted. (HE, 5X)

Contributor's Morphologic Diagnosis:
Heart: Severe regional cardiac myofiber vacuolar degeneration and glycogen accumulation.

Condition: Cardiac rhabdomyomatosis

Contributor's Comment:
The pathogenesis of this condition is still debated, though it is considered an incidental finding. Common features across veterinary species include the presence of PAS-positive material (interpreted as glycogen) within sarcoplasmic vacuoles and the formation of spider cells, which represent an artifact of glycogen loss during histologic processing.[4-10] Some sources attribute this condition to a defect in glycogen storage or metabolism.[3,9] An association with hypovitaminosis C

Cardiac Rhabdomyomatosis/Rhabdomyoma Cross-Species Comparison of Histochemical and IHC staining characteristics									
Species	Diagnosis	PAS	PTAH	Desmin	Myo-globin	SMA	Vimentin	PGP 9.5	NSE
Guinea pig (*Cavia porcellus*)	Cardiac rhabdomyomatosis	+	+	+	+	Variable			
Pig (*Sus scrofa*)	Cardiac rhabdomyoma	+	+	+			+	+	+
Canid (*Canis familiaris*)	Cardiac rhabdomyoma	+	+	+	+	-	-		
Bearded harbor seal *(Erignathus barbatus)*	Cardiac pukinjeoma	+	+					+	+
Fallow deer (*Dama dama*)	Cardiac rhabdomyoma	+	+	+			+		

(scurvy) has been suggested in guinea pigs, but is not well-established.[9]

Recent veterinary literature indicates that in swine, the abnormal myocytes contain ultrastructural and immunohistochemical features of both postnatal cardiac myocytes and Purkinje cells. These characteristics, in conjunction with the age predilection for juvenile animals, support the contention that this may represent a congenital dysplasia or a tumor arising from a pluripotent embryonic cell.[3,12] In humans, cardiac rhabdomyomas represent the most common primary pediatric cardiac neoplasm and, interestingly, are often associated with tuberous sclerosis complex.[5]

Contributing Institution:
Pathology Department
Charles River Laboratories – Mattawan

www.crl.com

JPC Diagnosis:
Heart, myocardium: Glycogenosis, multifocal, moderate.

JPC Comment:
This week's moderator was Major Daniel Bland, Chief of Histology (Veterinary Pathology) at the Walter Reed Army Institute of Research (WRAIR) and his cases were anything but mundane. This first entity is a classic in the guinea pig, though as the contributor also notes there are occasional case reports in other species as well. Recently, there was a short report of this condition in Göttingen Minipigs as well.[1] Tissue identification and lesion recognition was relatively simple for this case, so we focused on better characterizing the plump, atypical cardiac myocytes that the contributor so nicely describes/ Similar to the table provided, we ran IHCs and special stains for Periodic-Acid Schiff (with and without diastase), muscle specific actin, desmin, GFAP, IBA1, NSE, synaptophysin, and chromogranin. These atypical myocytes were

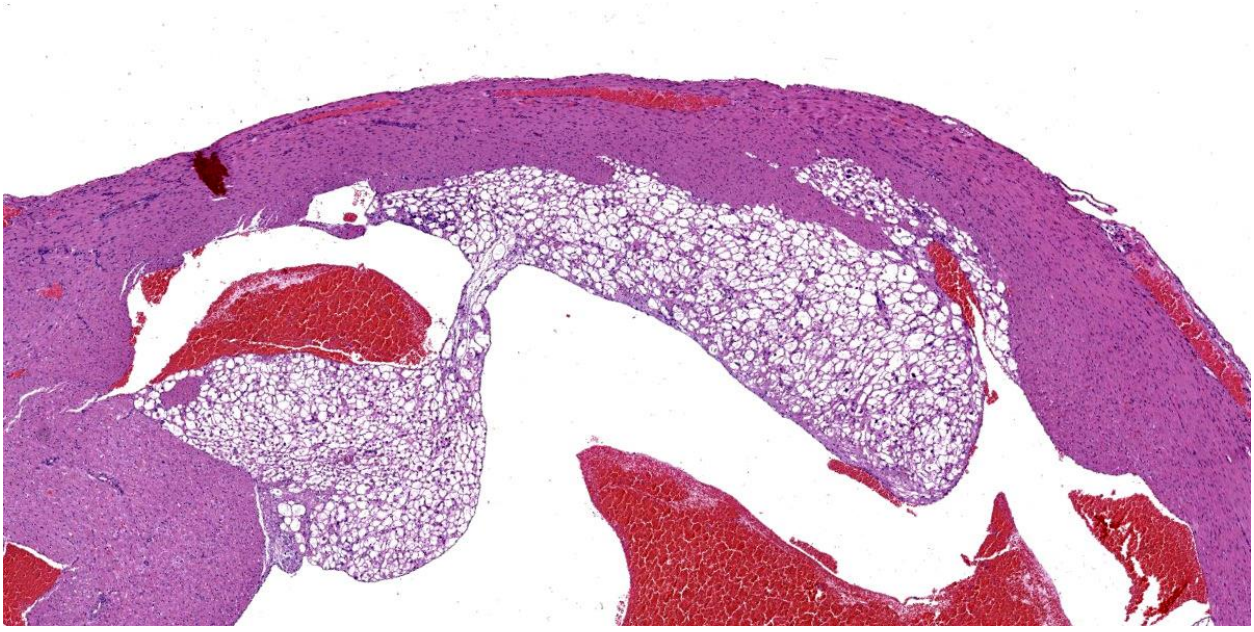

Figure 1-2. Heart, guinea pig. A focally extensive area of swollen cardiomyocytes is present within the right ventricle subjacent to the endocardium. (HE, 36X)

strongly PAS-positive within the cytoplasm, though this staining intensity was greatly diminished by treatment with diastase, consistent with interpretation of these vacuoles as containing glycogen. Compared with normal cardiac myocytes, these atypical myocytes also had minimal cytoplasmic immunoreactivity for desmin and muscle specific actin. Chromogranin and synaptophysin were immunonegative.

Conference participants had a few interesting takeaways from this case. Foremost, there was the observation that the PAS section following diastase treatment was quite washed out. As Dr. Bruce Williams reminded participants, cells with increased glycogen content include hepatocytes, neurons, and cardiac/skeletal myocytes – it is hardly a surprise then that the staining profile of these cells should change with this glycogen content also being digested. Participants also debated how to best describe this condition, with the consensus falling on a moderate severity given the limited ancillary changes within the heart (i.e. degeneration and necrosis of adjacent myocytes).

There are several other lesions to be aware of in the heart of guinea pigs which were not present in this case. These include rare mineralization of cardiac myocytes which may be accompanied by fibrosis and minimal mononuclear cell infiltration; alone this is typically subclinical.[9] Additionally, the underlying cause for myocardial protein aggregates in pet guinea pigs has been described,[11] with accumulation of these alpha B crystallin (a small heat shock chaperone protein) being most common in the right ventricular free wall, though they may also be found within papillary muscles within the left and right ventricles of the heart as well.

References:

1. Feller LE, Sargeant A, Ehrhart EJ, Balmer B, Nelson K, Lamoureux J. Cardiac Rhabdomyoma in Four Göttingen Minipigs. *Toxicol Pathol*. 2023 Jan;51(1-2):61-66.
2. Holley D, et al. Diagnosis and management of fetal cardiac tumors; a multicenter

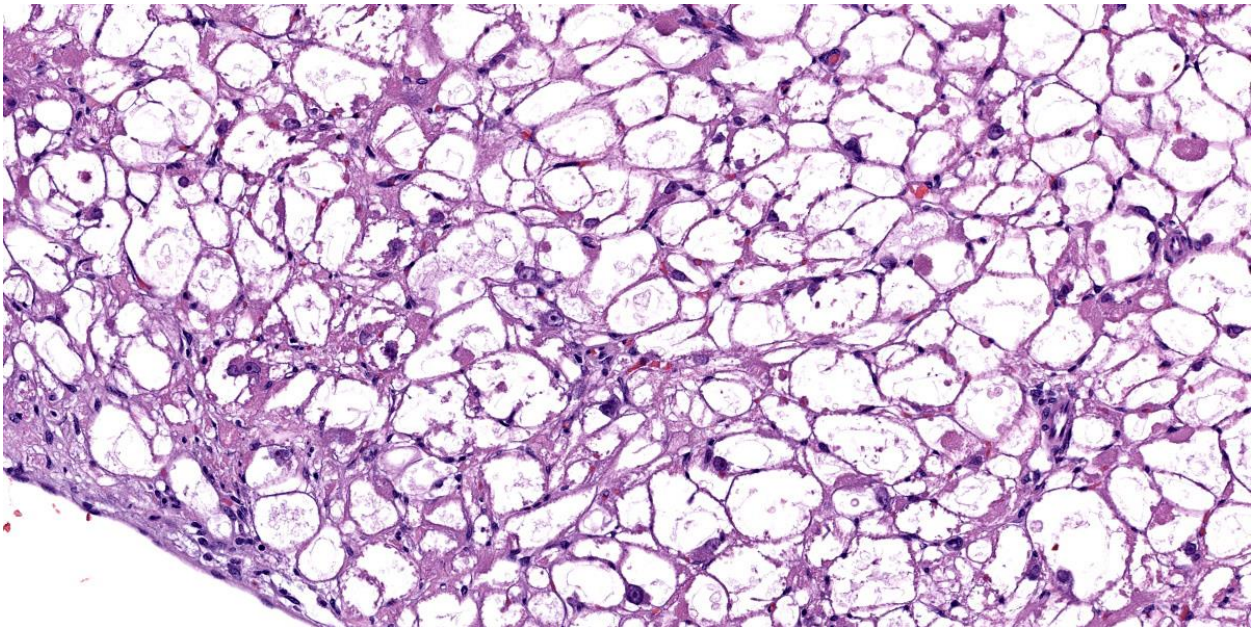

Figure 1-3. Heart, guinea pig. Cardiomyocytes are markedly expanded by glycogen forming "spider cells" (HE, 228X)

experience and review of published re ports. *J Am Coll Cardiol*, p. 516-520, 1995.

3. Jacobsen B, et al. Proposing the term purkinjeoma: Protein Gene Product 9.5 Expression in 2 Porcine Cardiac Rhabdomyoma Indicates Possible Purkinje Fiber Cell Origin. *Vet Pathol.* 2010;47(4):738-740.
4. Kizawa KK, et al. Cardiac rhabdomyoma in a Beagle dog. *Journal of Toxicologic Pathology*. 2002; 15(1):69-72.
5. Kobayashi TT, et al. A Cardiac rhabdomyoma in a guinea pig. *Journal of Toxicologic Pathology*. 2010;23(2):107-110.
6. Kolly C, et al. Cardiac rhabdomyoma in a juvenile fallow deer (Dama dama). *Journal of Wildlife Diseases*. 2004;40(3):603-606.
7. Krafsur G, et al. Histomorphologic and immunohistochemical characterization of a Cardiac Purkinjeoma in a Bearded Seal (Erignathus barbatus). *Case Reports in Veterinary Medicine*. 2014.
8. Pereira PA, et al. Cardiac rhabdomyoma in a slaughtered pig. *Cienc. Rural, Santa Maria.* 2018; 48(10):e20180460.
9. Percy DH, Griffey SM, and Barthold SW. *Pathology of Laboratory Rodents and Rabbits*. Ames, Iowa: Blackwell Pub, 2016, 241-242.
10. Radi ZA, Metz Z. Canine cardiac rhabdomyoma. *Toxicologic Pathology*. 2009;37(3):348-350.
11. Southard T, Kelly K, Armien AG. Myocardial protein aggregates in pet guinea pigs. *Vet Pathol*. 2022 Jan;59(1):157-163.
12. Tanimoto T, Ohtsuki Y. The pathogenesis of so-called cardiac rhabdomyoma in swine: a histological, immunohistochemical and ultrastructural study. *Virchows Archiv*. 1995;47(2):213-221.

CASE II:

Signalment:
Adult, male, Göttingen minipig, *Sus scrofa domesticus*

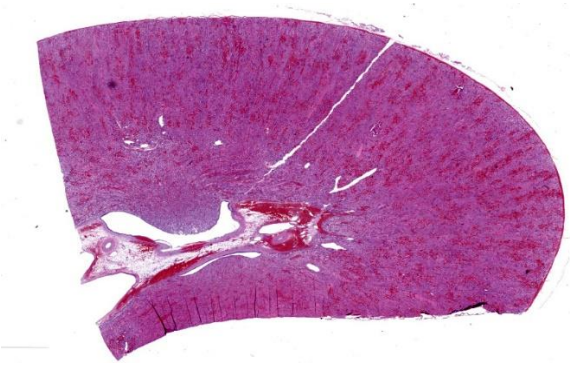

Figure 2-1. Kidney, Gottingen minipig. One section of kidney is submitted for examination. At subgross magnification, multifocal hemorrhage is present throughout the section. (HE, 4X)

History:
This source animal had an acute history of decreased activity, decreased appetite, and generalized orange-pink skin discoloration prior to initial test article administration. It was subsequently discovered laterally recumbent with an intermittent, abnormal breathing pattern. Bloodwork was collected immediately prior to euthanasia.

Gross Pathology:
There were no significant gross lesions.

Microscopic Description:
In the kidneys, renal tubules in the cortex and extending into the medulla are diffusely, mildly to moderately dilated and filled with eosinophilic proteinaceous fluid or erythrocytes. Epithelial cells lining effected tubules are multifocally flattened with basophilic cytoplasm and frequently contain hypereosinophilic, globular, cytoplasmic material. There are few scattered clusters of necrotic tubules within the cortex, characterized by hypereosinophilia, loss of differential staining, and nuclear pyknosis of the tubular epithelium. Occasionally, Bowman's spaces are dilated and filled with similar eosinophilic fluid and hypereosinophilic globular material which moderately compresses glomerular tufts. There is moderate, multifocal expansion of the renal interstitium and peri-pelvic adipose tissue by abundant hemorrhage which surrounds and separates renal tubules and adipocytes.

Contributor's Morphologic Diagnosis:
Kidney: Renal tubular hemorrhage and proteinosis, diffuse, acute, severe, with rare tubular degeneration and necrosis and diffuse interstitial hemorrhage

Contributor's Comment:
Histologic lesions are compatible with hemorrhagic syndrome in Göttingen minipigs, also known as thrombocytopenic purpura syndrome (TP). Hemorrhagic syndrome has been previously described in Göttingen minipigs with thrombocytopenia as the underlying cause.[1] Currently, the mechanism of the thrombocytopenia associated with hemorrhagic syndrome is unknown, but is thought to be secondary to an immune complex-associated disorder, specifically a type II-mediated thrombocytopenia and/or a type III-mediated vasculitis/glomerulonephritis.[1,7] Animals between 7 weeks and 1 year have been reported as affected with no apparent hereditary etiology.[1,6]

Clinically, pigs suffering from hemorrhagic syndrome are typically anemic and severely thrombocytopenic ($\leq$ 20,000/µl).[1,6] Depending on the severity of the disease and the organs affected, additional bloodwork abnormalities such as increased liver or renal values may be present, as in this case. Macroscopically, widespread hemorrhage is a key feature in hemorrhagic syndrome, including petechial to ecchymotic hemorrhages or hematomas most commonly observed in the skin, heart, urinary bladder, and kidney.[7] While there were no discrete hemorrhages observed macroscopically in this case, the generalized orange to pink skin discoloration and hyperbilirubinemia suggest that there was significant hemolysis in this animal.

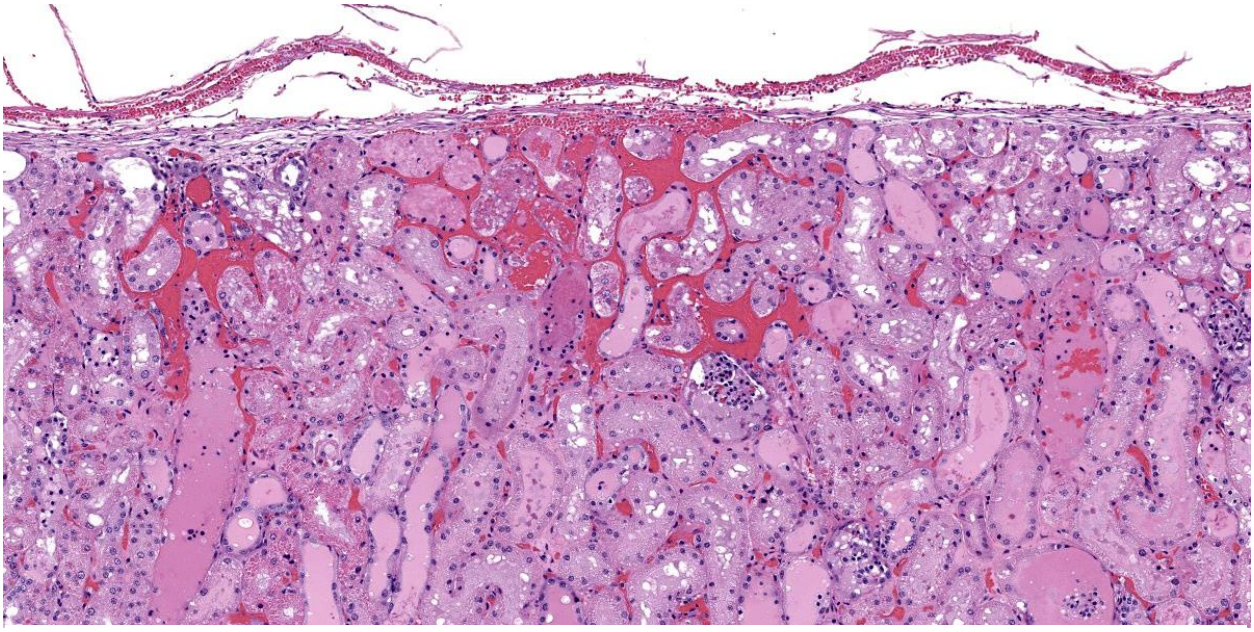

Figure 2-2. Kidney, Gottingen minipig: In this subcapsular field, there is multifocal acute hemorrhage, with tubular epithelial degeneration and necrosis. (HE, 294X)

Microscopically, lesions of hemorrhagic syndrome consist of multifocal interstitial to mucosal hemorrhages in multiple organs including but not limited to the skin, kidney, bladder, intestine, pancreas, lymph nodes, lungs, and skeletal musculature.[1,7] In the kidneys, membranoproliferative glomerulonephritis is a common feature, characterized by thickening of glomerular basement membranes and an increase in the number of mesangial cells within glomerular tufts.[1,6] Degenerative and proliferative vascular lesions affecting small to medium-sized muscular arteries and arterioles have also been reported in cases of hemorrhagic syndrome.[6] Previously described vascular lesions range from endothelial cell hypertrophy and smooth muscle cell vacuolation to proliferation of the tunica intima, necrosis and thickening of the tunica media, and disruption of the internal elastic membrane.[6] These lesions can also be accompanied by lymphohistiocytic to neutrophilic periarteritis.[6] Vascular lesions are most commonly observed in the heart and renal pelvis, but can found in other affected tissues.[6]

Based on the rapid progression of clinical signs, lack of significant gross lesions and microscopic evidence of hemorrhage in the kidney, this case is considered to represent a peracute presentation of hemorrhagic syndrome in the Göttingen minipig. Certain histologic lesions typically observed in TP, such as hemorrhages in multiple organs and appreciable membranoproliferative changes in the kidney, were not present in this case, but may have developed later in the course of disease had this animal not been euthanized. The hypereosinophilic, globular material observed in the cytoplasm and lumen of renal tubules has been previously reported in cases of hemorrhagic syndrome and, in those cases, was confirmed to be IgG, IgM or C1q with immunohistochemistry, supporting an immune-mediated cause for the disease.[1]

Some differentials to consider for hemorrhagic syndrome in Göttingen minipigs include other hemorrhagic disorders such as neo-natal alloimmune thrombocytopenia and von Willebrand disease (VWD). Neonatal alloimmune thrombocytopenia occurs in piglets

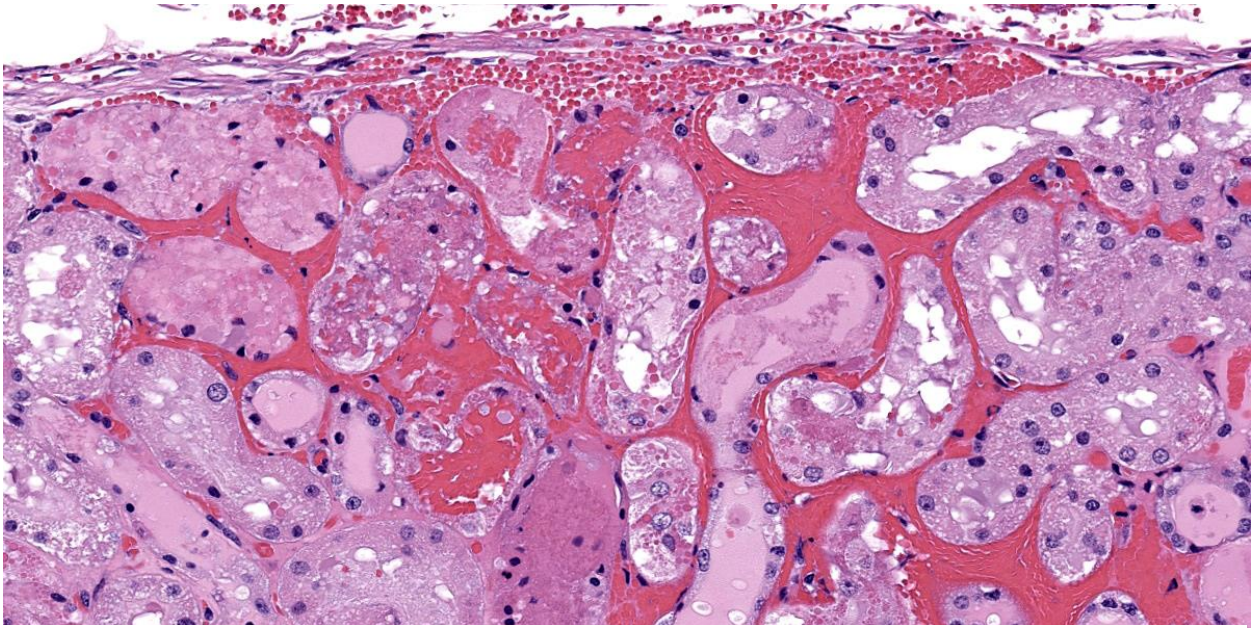

Figure 2-3. Kidney, Gottingen minipig. Higher magnification of the field in Fig. 2-2, with tubular degeneration and necrosis (HE, 294X).

less than a week old and is associated with immune-mediated platelet destruction by alloantibodies produced in sow colostrum against fetal platelet antigens inherited from the boar.[2] Von Willebrand disease is a dominant recessive, hereditary bleeding disorder caused by a mutation in von Willebrand factor.[5] Type 3 VWD, the most severe form of the disease in which there is a near total absence of von Willebrand factor, has been previously reported in farm pigs and causes severe mucocutaneous and periarticular hemorrhage that can be fatal if not treated.[5] While petechial to ecchymotic hemorrhages can occur virtually anywhere with hemorrhagic syndrome and may present similar to VWD grossly, VWD does not commonly cause visceral hemorrhages and has not been reported to cause membranoproliferative changes in the kidney.

Contributing Institution:
Charles River Laboratories, Mattawan, MI
www.crl.com

JPC Diagnosis:
Kidney: Hemorrhage, acute, multifocal to coalescing, marked with tubular degeneration, necrosis, regeneration, and proteinosis.

JPC Comment:
Case 2 ratchets up the pathology seasoning nicely, with our case discussion being particularly spicy. In this case, the widespread hemorrhage within the renal interstitium is an obvious feature, though the tubular changes should not be overlooked (Figures 2-2, 2-3, and 2-4). As this animal was euthanized and quickly necropsied, the cellular preservation of this section is excellent which negates the frustration of reading through autolytic changes. We agreed with the contributor that the hemorrhage noted fits with an acute interpretation of this lesion, though some participants quibbled that a true 'peracute' lesion would have no supporting histologic features as the animal would succumb too quickly. This however was the easy part of the case discussion.

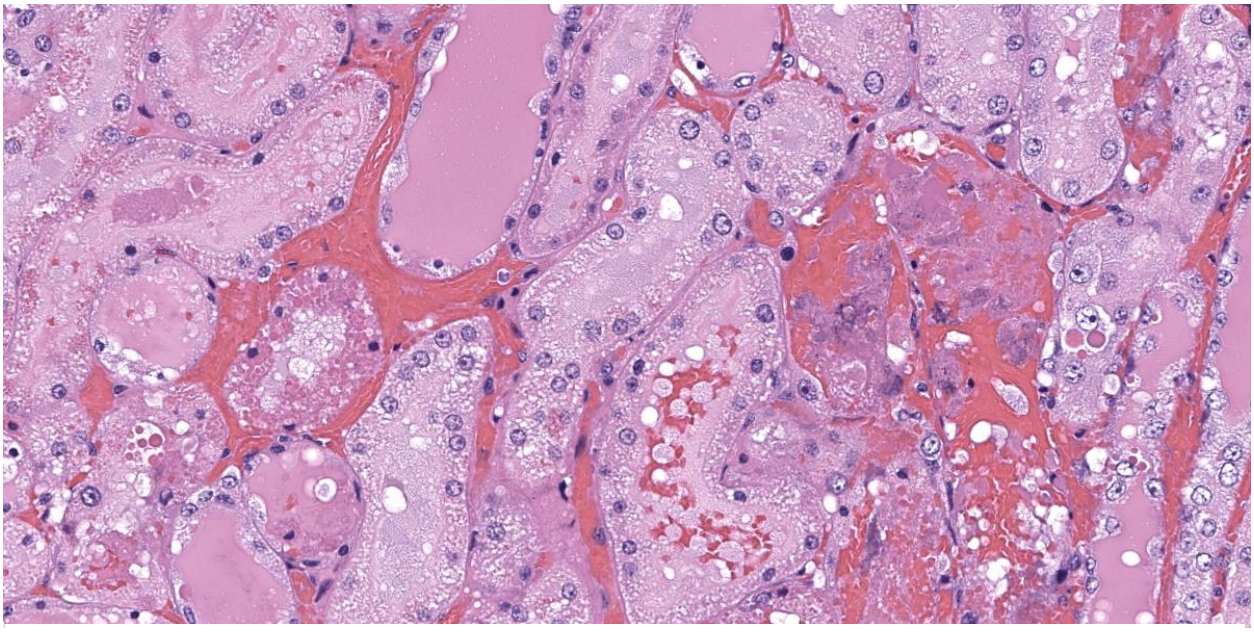

Figure 2-4. Kidney, Gottingen minipig. More tubular degeneration and necrosis within tubules. Numerous tubules contain abundant luminal protein. (HE, 314X)

Interestingly, a number of conference participants also raised the question of whether there could be underlying chronic changes in this case which we catalog in detail. Participants felt strongly that thrombocytopenic purpura syndrome would likely have some supporting chronic changes given the pathogenesis the contributor describes. We last saw this entity in Conference 3 in 2023-2024, though there are some key differences to note. In last year's case, we reviewed multiple sections from the ear that featured arteriosclerosis with modest arteritis and periarteritis, including thrombi in section. In this case, there are some small- and medium-caliber blood vessels near the renal pelvis/hilus (figure 2-1) that have medial hypertrophy of the tunica media ('onion-skinning') with endothelial hypertrophy. Additionally, some participants noted rare foci of basophilic renal tubular cells that were stacked and had mitotic figures (interpreted as regeneration) which would support a chronic interpretation of this lesion. Within the collecting ducts, there are also multiple granular casts present which points towards a longer time course in this case as well. We looked carefully for ancillary changes that would align with this interpretation and ran both PAS and JMS (Jones Methenamine Silver) to highlight the glomerular basement membrane as well as a Movat's pentachrome to examine the wall of blood vessels. We agree with the contributor that there were no glomerular changes in this case to include thickening of the basement membrane, discontinuity or deposits within the membrane, or any glomerular synechiae in any of the sections examined. Movat's stain did show discontinuity of both the inner and outer elastic lamina in select vessels which was not readily apparent on H&E section. Nonetheless, we struggled to find a good example of vasculitis on our section as the lack of vascular change (vascular necrosis and/or surrounding inflammation) or obvious fibrin thrombi made it difficult to pin down the exact connection to the large degree of hemorrhage and subsequent tubular change in this animal. This could be related to thrombocytopenia, though we did wonder about the nature of the perimortem blood sample clotting and its relation to this case too. With these features in

mind, we cautiously approached the morphological diagnosis for this case, and focused only on the features that we felt we had solid support for histologically. We thank the contributor for submitting this case as it prompted a fruitful discussion here at the JPC.

There are a number of potential rule outs for acute tubular injury and hemorrhage in swine. These include porcine circovirus (dermatitis and nephropathy syndrome), porcine respiratory and reproductive syndrome virus, classical swine fever, African swine fever, septicemia, and anticoagulant rodenticide ingestion.[3] For Göttingen minipigs, background renal lesions are fairly limited and mild, and did not confound interpretation of this case.[4]

References:

1. Carrasco L, et al. Immune complex-associated thrombocytopenic purpura syndrome in sexually mature Göttingen minipigs. *J Comp Pathol*. 2003 Jan;128(1):25-32.
2. Forster LM. Neonatal alloimmune thrombocytopenia, purpura, and anemia in 6 neonatal piglets. *Can Vet J*. 2007 Aug;48(8):855-7.
3. Imai DM, Cornish J, Nordhausen R, Ellis J, MacLachlan NJ. Renal tubular necrosis and interstitial hemorrhage ("turkey-egg kidney") in a circovirus-infected Yorkshire cross pig. *J Vet Diagn Invest*. 2006 Sep;18(5):496-9.
4. Jeppesen G, Skydsgaard M. Spontaneous background pathology in Göttingen minipigs. *Toxicol Pathol*. 2015 Feb;43(2):257-66.
5. Lehner S, et al. A 12.3-kb Duplication Within the VWF Gene in Pigs Affected by Von Willebrand Disease Type 3. *G3 (Bethesda)*. 2018 Feb 2;8(2):577-585.
6. Maratea KA, Snyder PW, Stevenson GW. Vascular lesions in nine Göttingen minipigs with thrombocytopenic purpura syndrome. *Vet Pathol*. 2006 Jul;43(4):447-54.
7. Skydsgaard M, et al. International Harmonization of Nomenclature and Diagnostic Criteria (INHAND): Nonproliferative and Proliferative Lesions of the Minipig. *Toxicol Pathol*. 2021 Jan;49(1):110-228.

CASE III:

Signalment:
17-year-old, intact female, rhesus macaque, *Macaca mulatta*, Non-human primate (NHP)

History:
This NHP was part of several animals who lived in a research colony in Texas for several years prior to being transported to Maryland. The animal had recently become very unthrifty with a very poor body condition. Due to a worsening condition, humane euthanasia was elected.

Gross Pathology:
The heart was diffusely enlarged up to 1.5 times the normal size and bilaterally the ventricular free walls were thin and flabby. The pericardium contained approximately 75 mL of serosanguineous fluid. In the left ventricle, there were multiple white nodules adhered to the endocardium. The serosal surfaces of the small and large intestines were reddened. The liver had a diffuse cobblestone appearance. The gallbladder was markedly enlarged up to three times normal. The splenic capsule had a diffusely nodular appearance. The right adrenal gland had a single, tan, 2 mm nodular lesion in the cortex. There was approximately 50 mL of serosanguineous fluid in the thorax and 50 mL of similar fluid in the abdomen.

Laboratory Results:
Biochemistry profiles showed chronically elevated liver and kidney values with low protein. Exact values were unavailable. PCR testing on formalin-fixed cardiac tissue was positive for *Trypanosoma cruzi*.

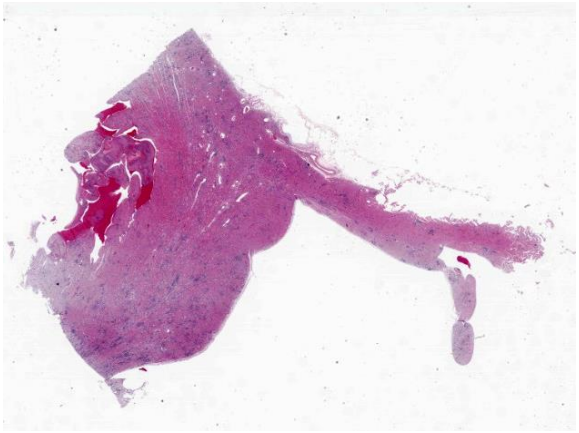

Figure 3-1. Heart, macaque. One section of heart including the base of the left and right ventricle and the interventricular septum is submitted for examination (HE, 5X)

Microscopic Description:
Diffusely and transmurally affecting approximately 60% of the section, large numbers of inflammatory cells composed of macrophages, lymphocytes, plasma cells, and neutrophils with fibroblasts surround, infiltrate, and replace cardiomyocytes. Cardiomyocytes adjacent to these inflammatory cells are often degenerate characterized by swollen, pale and vacuolated sarcoplasm or are necrotic characterized by hypereosinophilic sarcoplasm with loss of cross striations, and fragmentation of the nucleus with cellular and karyorrhectic debris. Multifocally within cardiomyocytes are numerous pseudocysts measuring up to 40 um x 90 um which contain a plethora of 2-4 um protozoal amastigotes with a basophilic nucleus and kinetoplast. Fibrin, hemorrhage, and edema is also present in these inflammatory regions. Present within the left ventricular lumen are multiple enmeshed clots adhered to the papillary muscles composed of fibrin, hemorrhage, edema, and similar inflammatory cells.

Contributor's Morphologic Diagnosis:
Heart: Panmyocarditis, histiocytic and lymphoplasmacytic, chronic, diffuse, severe, with myocardial degeneration, necrosis, and loss, and intramyocytic protozoal amastigotes, rhesus macaque, non-human primate.

Contributor's Comment:
The histopathologic findings and PCR test results are diagnostic for cardiac trypanosomiasis caused by *Trypanosoma cruzi*. *T. cruzi* is the causative agent for Chagas disease, otherwise known as American trypanosomiasis. Trypanosomes are hemoflagellate protozoans known to infect humans and a variety of domestic and wild animals throughout North and South America. In the southern United States, opossums, raccoons, and armadillos serve as the primary reservoir hosts.[1,3,5,7]

T. cruzi is most commonly spread through stercorarian transmission when its vector, the triatomine bug (also called the reduviid or kissing bug), defecates or urinates trypomastigotes of *T. cruzi* at the site of a recent blood feeding. Trypomastigotes from the feces or urine enter the wound and disseminate hematogenously to cardiomyocytes. Trypomastigotes invade cardiomyocytes where they develop within the sarcoplasm into amastigotes within a pseudocyst. After replication, the amastigotes mature into trypomastigotes, rupture the host cell, and re-enter systemic circulation. This infective form is then ingested by a triatomine bug during a blood feeding where it transforms into an epimastigote in the insect's gut and replicates through binary fission while awaiting the cycle to begin anew.[1,3,5,7,8] While the heart is the primary organ affected, amastigotes have also been identified in several other organs.[3] In this case, a pseudocyst was also identified in the diaphragm. Additional documented forms of transmission include oral ingestion of the vector or contaminated feces, transplacental and transmammary transmission, blood transfusions, and organ transplantation.[1,5,8]

Classic clinical and pathologic findings follow a pattern of cardiac disease. In the acute phase,

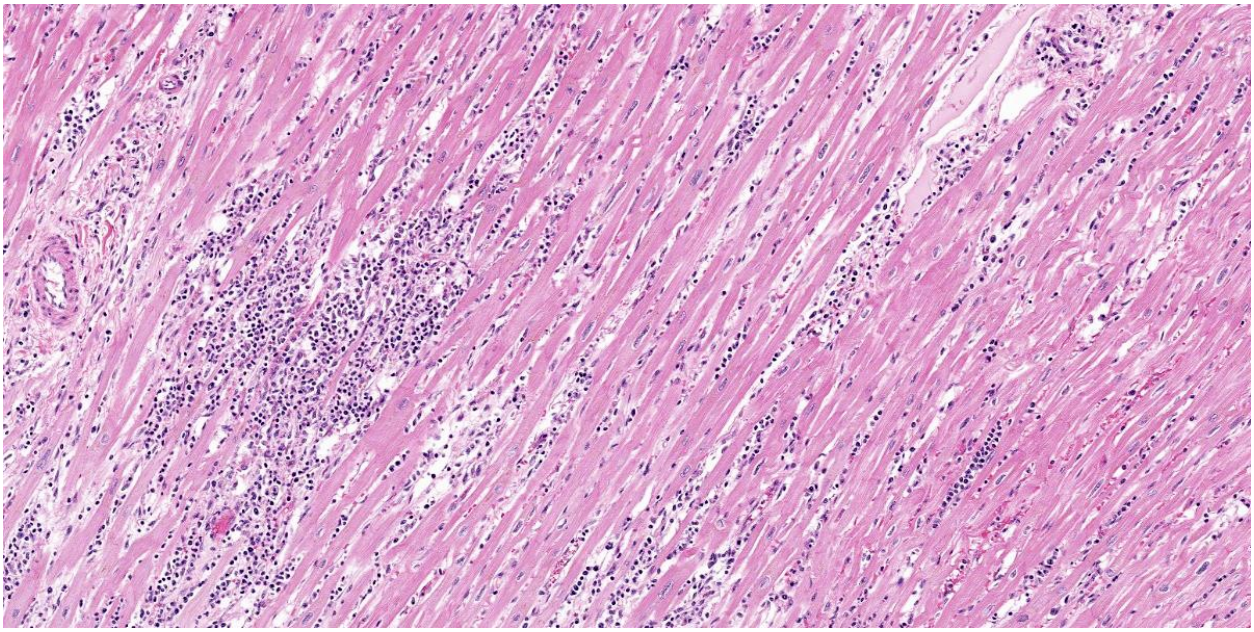

Figure 3-2. Heart, macaque. Multifocally throughout the section, there are large aggregates of macrophages, lymphocytes, and plasma cells with surround, separate and replace cardiomyocytes. (HE, 118X)

cardiac arrhythmias, sudden collapse, or even death, weak pulses, and signs of respiratory distress can all be expected. Animals that survive the acute phase can anticipate developing chronic heart disease. Cardiac dilatation is common as are more frequent cardiac arrhythmias and clinical signs consistent with unilateral or bilateral heart failure.[3]

Cytology of blood smears during the acute phase can be used to identify trypomastigotes present in the systemic circulation. In the chronic phase when parasitemia is lower, a thick-film buffy coat smear should be used to increase the concentration of the organisms. Lymph node aspirates and cytologic analysis of abdominal effusion has also been documented to identify *T. cruzi*. Serologic and molecular testing has also been useful in premortem diagnosis.[5]

Post-mortem findings will vary depending on if the animal died during the acute or chronic phase of infection. Lesions from death during the acute phase include a pale myocardium with hemorrhages in the subendocardial and subepicardial surfaces. Right-sided heart lesions are often more severe than the left side. Generalized lymphadenopathy has also been reported. Chronically infected animals often present with generalized cardiomegaly with thinning of the ventricular free walls and a serosanguineous fluid in the pericardial, pleural, and abdominal cavities. Microscopic findings include multifocal to diffuse histiocytic to lymphoplasmacytic myocarditis with varying stages of cardiomyocyte degeneration and necrosis with fibrosis. The presence of intracardiomyocytic amastigotes is a very helpful but can be difficult to find especially in chronic cases.[1,5]

A recent study documenting the histologic findings of *T. cruzi* in domestic cats documented lymphoplasmacytic myocarditis with fibrosis in 42.1% of seropositive cats compared to 28.6% of seronegative cats. In the same study, PCR for *T. cruzi* was performed on a variety of tissues from seropositive and seronegative cats. PCR-positive tissues included heart, biceps femoris muscle, sciatic nerve, esophagus, and mesentery.[8] Although

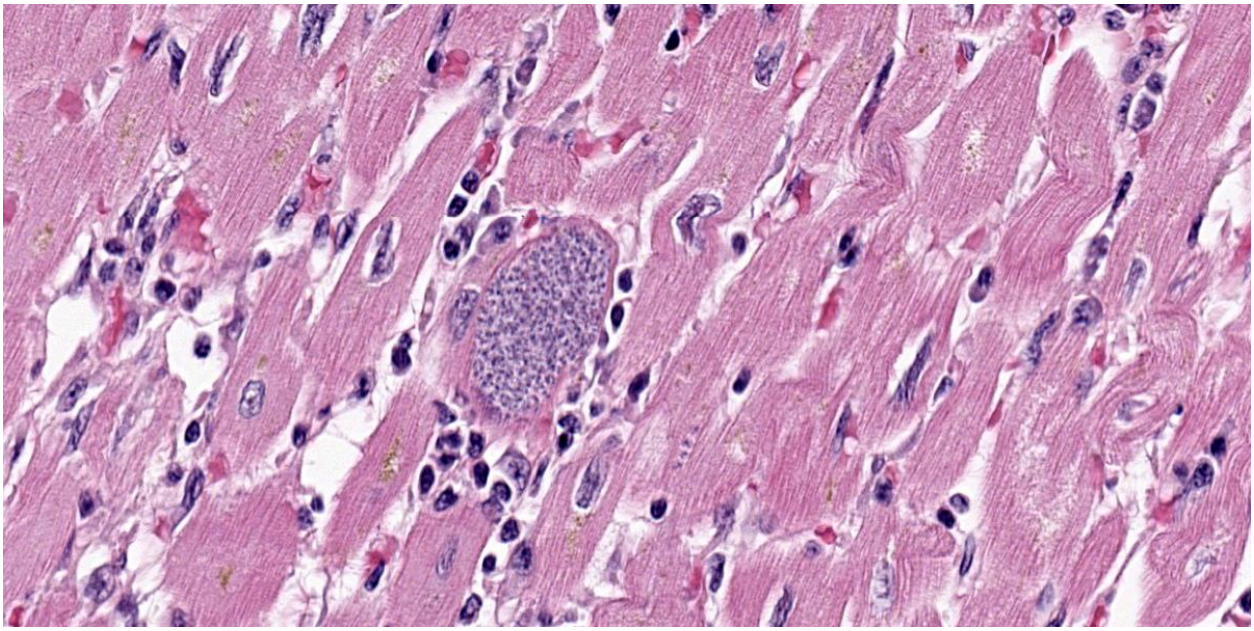

Figure 3-3. Heart, macaque. Occasionally cardiomyocytes contain a large cytoplasmic pseudocyst containing numerous 2-3um round trypanosomal amastigotes with a central nucleus and poorly discernable kinetoplasts. (HE, 727X)

CNS disease is considered an uncommon manifestation of *T. cruzi* infection in non-human mammals, disseminated trypanosomiasis with central nervous system (CNS) involvement was recently reported in four dogs, with CNS involvement confirmed by quantitative PCR. Lymphohistiocytic myocarditis and histiocytic meningoencephalitis with rare to numerous intralesional and intracellular amastigotes were reported in all 4 dogs, while gross lesions within the CNS were observed in 2/4 dogs.[3]

Contributing Institution:
Walter Reed Army Institute of Research; Department of Pathology;
https://www.wrair.army.mil/

JPC Diagnosis:
Heart: Pancarditis, lymphoplasmacytic and histiocytic, chronic, multifocal to coalescing, marked, with fibrosis and numerous intrmyocytic amastogotes.

JPC Comment:
At first glance, this section of heart is nondescript save for the random, coalescing regions of basophilia (Figure 3-1) that represent the inflammatory cells in the myocardium that the contributor describes. On higher magnification however, there are a plethora of changes occurring in this case that provide some zest to the pathology palate. To wit, we ran special stains (Giemsa, PTAH, Masson's trichrome) for this case and they did not disappoint. The degree of fibrosis in this case is not surprising given the loss of cardiac myocytes secondary to both rupture of amastigote-laden cells and the marked inflammatory response (figures 3-2 and 3-3), though cardiac fibrosis can also be a background lesion in aged macaques. In this case, trypanosomal amastigotes were obvious on H&E, though they were also highlighted metachromatically by Giemsa with the kinetoplasts being a sharp red against the medium blue background. We also ran a modified

Gram stain (Brown-Brenn, Brown-Hopps) and fungal stains (GMS, PAS Light Green) which did not identify any concurrent infections in this animal. Although tinctorially similar to the myofibers, there are also two fibrin thrombi nestled within the ventricle as the contributor points out. Conference participants overall liked the quality of this slide and the descriptive features as they felt they were rewarding to discuss.

Natural infection of non-human primates with Chagas disease has been described in the veterinary literature previously. [2,4,6] Given the preponderance of primate facilities in Texas similar to where the animal in this case originated, discussion of trypanosomiasis and its impacts on medical research remains relevant. A similar case of trypanosomal myocarditis in a rhesus macaque was previously covered in Conference 17, Case 2, 2013-2014.

Finally, another important rule out for this case is leishmaniasis which appears nearly identically to trypanosomes histologically. In theory, the orientation of the kinetoplast (parallel to the nucleus for trypanosomes, perpendicular for *Leishmania*) might help to discriminate these entities, though PCR is preferable if available. The advancing range of reduviid bugs has implications on animal and human health that are not lost on us at the JPC. Given that the Department of Defense's Military Working Dog Program is anchored in San Antonio, Texas[6], we see several cases of canine trypanosomiasis each year when such cases were rarer previously. Given worldwide deployment of Military Working Dogs, discerning *T. cruzi* infection against other agents remains an important task.

References:

1. Boes KM, Durham AC. Bone marrow, blood cells, and the lymphoid/lymphatic system. In: McGavin MD, Zachary JF, eds. *Pathologic Basis of Veterinary Disease*. 7th ed. St. Louis, MO: Elsevier; 2022:834.
2. Hodo CL, Wilkerson GK, Birkner EC, Gray SB, Hamer SA. Trypanosoma cruzi Transmission Among Captive Nonhuman Primates, Wildlife, and Vectors. *Ecohealth*. 2018 Jun;15(2):426-436.
3. Landsgaard K, et al. Protozoal meningoencephalitis and myelitis in 4 dogs associated with *Trypanosoma cruzi* infection. *Vet Pathol*. 2023;60(2):199-202.
4. Rovirosa--Hernández MJ, López-Monteon A, García-Orduña F, et al. Natural infection with Trypanosoma cruzi in three species of non-human primates in southeastern Mexico: A contribution to reservoir knowledge. *Acta Tropica*. 2021;213:105754.
5. Snowden KF, Kjos SA. American trypanosomiasis. In: Greene CE, ed. *Infectious Diseases of the Dog and Cat*. 4th ed. St. Louis, MO: Elsevier-Saunders; 2012:722-30.
6. Tarleton R, Saunders A, Lococo B, et al. The Unfortunate Abundance of Trypanosoma cruzi in Naturally Infected Dogs and Monkeys Provides Unique Opportunities to Advance Solutions for Chagas Disease. *Zoonoses*. 2024;4(10).
7. Valli VEO, Kiupel M, Bienzle D. Hematopoietic system. In: Maxie MG, ed. *Jubb, Kennedy, and Palmer's Pathology of Domestic Animals*. Vol 3. 6th ed. Philadelphia, PA: Saunders Elsevier; 2016:121-124.
8. Zecca IB, et al. Prevalence of *Trypanosoma cruzi* infection and associated histologic findings in domestic cats (*Felis catus*). *Vet Parasitol*. 2020;278:109014.

Figure 4-1. Oral cavity, rhesus macaque. A 4 x 2 cm mass extends from the caudal aspect of the hard palate into the soft palate and pharynx (arrow). The mass was soft with an irregular surface that was mottled light and dark gray. (*Photo courtesy of:* NIH, 9000 Rockville Pike, Building 28A, Room 117, Bethesda, MD 20892)

CASE IV:

Signalment:
18 year-old, male, rhesus macaque, Macaca mulatta

History:
During a physical examination, a mass was found at the back of the mouth and was biopsied. A week later, based on the biopsy result, the monkey was euthanized.

Gross Pathology:
A 4 x 2 cm mass extended from the caudal aspect of the hard palate into the soft palate and pharynx. The mass was soft with an irregular surface that was mottled light and dark gray. The draining lymph nodes appeared to be enlarged. Photo of fixed tissue: arrows delineate the extension of the mass from the ulcerated hard palate into the pharynx.

The liver was markedly enlarged and diffusely pink and had a white texture on cut section. Along the apical margins of the liver were white well demarcated firm foci that also were waxy in texture. Lungs, heart, spleen, kidneys and GI were grossly normal.

Microscopic Description:
Moderately pleomorphic neoplastic cells expanded the submucosa and extended to the cut edges of the sections. The cells were round to oval to stellate and ranged in size from 15-50um. Nuclei were round to oval and had prominent nucleoli. Cells had abundant wispy cytoplasm with small vesicles and a few had faint brown pigment granules. Mitoses averaged 2/HPF although some fields had as many as 5 mitotic figures. Some of the mitoses had an unusual appearance. In addition, hyphae consistent with candida and bacterial cocci were present in ulcerated areas [not present in all slides]

Submandibular lymph nodes were largely effaced by similar cells. A section of lung had microscopic metastasis.

Liver: The liver had severe amyloidosis with tumorous deposits at the apical margins. Heart, spleen, kidney and salivary glands were normal.

Special stains:
Fontana-Masson: biopsy, tumor, and lymph node had scattered positive cells.
Giemsa: (-)

Immunohistochemistry**:**
S-100, SOX-10, Melan A, PNL, HM45: (+)
Cytokeratin AE1/AE3: (-)

TEM: One percent of the tumor cells were positive for melanin and `contained 1 to 50 granules. All four stages of melanin granules were present with stages 3 and 4 predominating. The enclosed image shows all four stages.

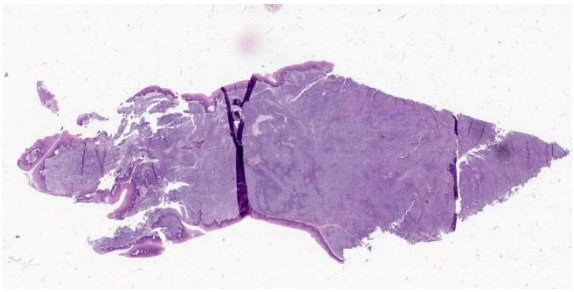

Figure 4-2. Oral cavity, rhesus macaque. A superficial section of the mass is submitted for examination. Neoplastic cells efface the lamina propria and extend to the overlying mucosal epithelium. (HE, 9X)

Contributor's Morphologic Diagnosis:
Amelanotic melanoma

Contributor's Comment:
Melanocytes arise from neural crest cells and reside not only in the basal cells of the epidermis and hair follicles, but also the eyes and meninges. Melanin synthesis occurs in melanosomes, lysosome-like organelles in melanocytes. Two major melanin pigments synthesized are pheomelanin (red/yellow in color) and eumelanin (brown/black). Both pigments arise from L-tyrosine which, when acted upon by tyrosinase, leads to DOPA (dihydroxyphenylalanine) formation. Production of DOPA from L-tyrosine is the rate limiting step in melanogenesis.[3] Oxidation and polymerization of DOPA leads to the formation of pheomelanin. Further enzymatic action by tyrosinases produces eumelanin. The percentage of eumelanin and pheomelanin determines the color of the skin/hair.[3,5]
Packaging of melanin into melanosomes occurs in four identifiable stages as seen by electron microscopy. Early melanosome stages I and II do not contain melanin but fibers formed during these stages give melanosomes their ovoid shape. Deposition of melanin begins in stage III and completely fills the melanosome in stage IV melanosomes.[5] Once formed, melanosomes are transferred to keratinocytes and are moved into the supranuclear area to form melanin caps which protect nuclei against UV damage. Melanin degrades as keratinocytes undergo squamous maturation.[3,5]

Melanoma is called the "great imitator" as the cells can have epithelioid, spindloid, clear, signet ring–like, myxoid, desmoplastic, rhabdoid, ballooning, and plasmacytoid forms.[7,9,10] Additional features of melanoma include high mitotic rate, unusual morphology of mitotic figures and the presence of junctional change by neoplastic cells.[6,12]

Some common stains used for diagnosis are Fontana-Masson which stains melanin granules brown in tumors that have little pigmentation. Bleach clears melanin in deeply pigmented tumors to examine the morphology of the cells. Giemsa is another stain to rule out mast cell tumors

Since melanomas, and other pigmented masses, may express more than one marker and immunohistochemistry can stain more than one cell type, including non-neoplastic cells, "cocktails" of markers are used to make diagnoses, identify micrometastases in sentinel lymph nodes, determine prognosis, and develop treatment strategies.[2,3,7] Specific markers include:

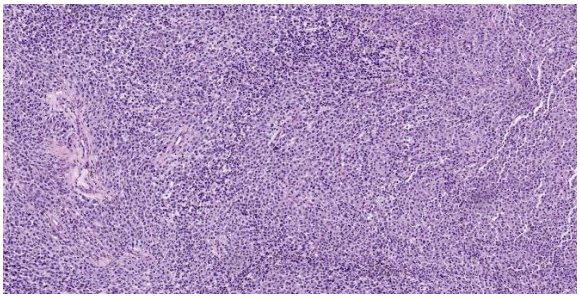

Figure 4-3. Oral cavity, rhesus macaque. Neoplastic round cells are arranged in sheets (HE, 91X)

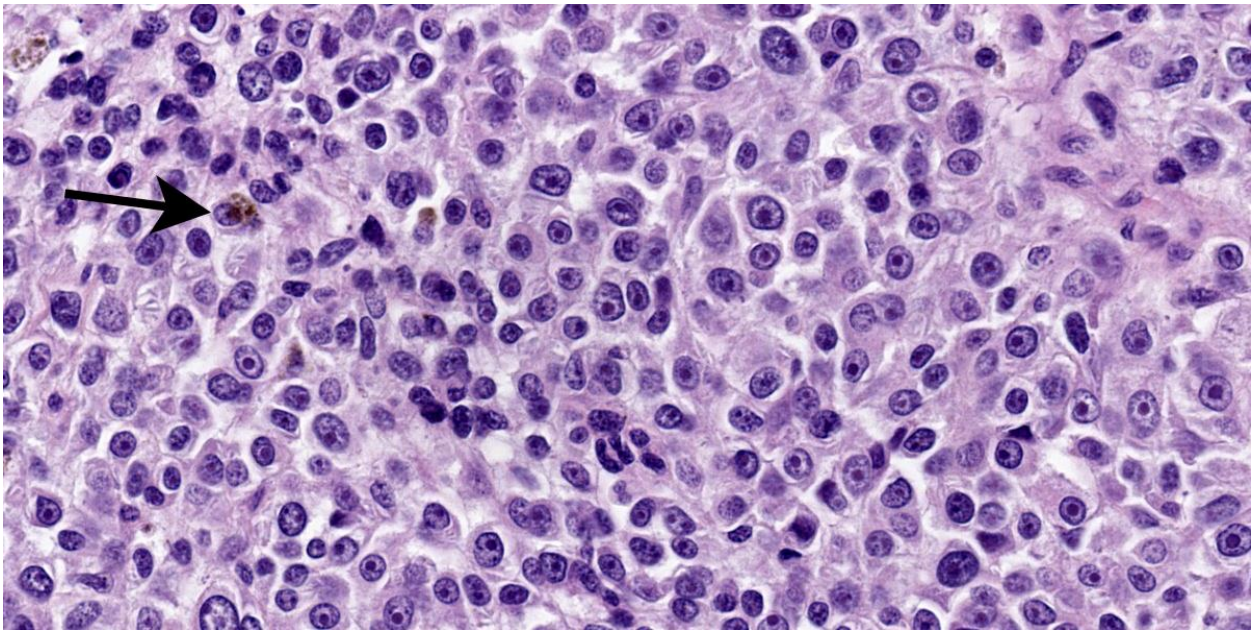

Figure 4-4. Oral cavity, rhesus macaque. Neoplastic cells have round nuclei with prominent nucleoli and few cells contain cytoplasmic melanin (arrow). (HE, 581X)

Cytokeratin: expressed in epithelial origin tumors.

S-100: is expressed in all subtypes of melanoma and identifies cells derived from the neural crest.[7] S-100 may also be expressed in other tumors.

Melan-A: (aka melanoma-associated antigen recognized by T cells) plays an important role in the formation of stage II melanosomes which have structural proteins.[2,7]

MITF: (microphthalmia-associated transcription factor) is the central regulator of melanogenesis. It is essential for melanocyte development and regulates genes for melanogenesis, cell survival, and differentiation.[3,7] MITF stain is sensitive but not specific. It is used as part of a cocktail because the staining pattern is nuclear and most other stains are cytoplasmic.[3,7]

HMB-45: (human melanoma black) is associated with the structural organization of melanosomes and with the fibrillar matrix and the maturation in stages I to II melanocytes.[7]

SOX10: (sry-related HMg-box gene10) is a nuclear transcription factor that regulates the differentiation of neural crest progenitor cells into melanoblasts and melanocytes.[3,7]

A pigmented, perioral melanoma with metastases to the lymph nodes, lung, liver, and kidney has been reported in a mountain gorilla.[4] Oral melanoma has not been reported in macaques and reports of melanoma involving other sites are rare. There is one report of melanoma in the choroid with no metastases in a cynomolgus macaque[1] and one report of cutaneous melanoma with metastases to local lymph nodes, also in a cynomolgus macaque.[8]

In humans, melanoma can be separated into three categories based on the amount of sun exposure: high cumulative sun damage, low cumulative sun damage and sun protected. Sun protected areas are further divided into acral (i.e. palms of the hands, soles of the feet, and the nails), mucosal/genital, uveal and CNS. The type and number of mutations can vary based on the location of the primary tumor.[2,13]

Figure 4-5. Oral cavity, rhesus macaque. Neoplastic melanocytes demonstrate multiple stages of melanosomes, ranging from Stage 1 (lightest) to Stage 4 (darkest). (TEM, 5000k)

While the incidence of cutaneous melanoma has increased over the last 50 years, the incidence of mucosal melanoma has remained fairly constant.[2,13] Mucosal membrane melanomas are rare and are more aggressive with a less favorable outcome compared to cutaneous melanomas. The low survival rate is due to lack of clinical signs and the likelihood that melanoma has already spread to local lymph nodes at the time of diagnosis.[2,9,12] In addition to local lymph nodes, melanoma tends to metastasize to the lungs and liver.[2,13]

Malignant melanoma has been reported to develop in a variety of mammalian and nonmammalian species including dog, rabbit[14], shark, parrot, pig and monkey.[2,13] In the dog, malignant melanoma is the most common oral tumor[9], is locally aggressive and tends to metastasize to local lymph nodes and lung.[9,10] Breeds that are more likely to develop oral melanoma are Poodle, Golden and Labrador retrievers, Rottweilers and Yorkshire terriers.[9]

Some aspects of canine oral melanoma are similar to humans. In both, the etiology is unknown, clinical course is aggressive and definitive treatment for oral melanoma is lacking.[2,9] The appearance of the neoplastic cells is variable and combinations of immunohistochemistry markers are used to diagnose the subtype of melanoma more definitively.[7,9] For example, a cocktail of Melan-A, PNL2, TRP-1(tyrosinase related protein-1), and TRP-2 (tyrosinase related protein-2) has been found to be useful in the diagnosis of amelanotic melanoma in dogs.[10]

Treatment may include surgical excision, radiotherapy, and chemotherapy but none have been particularly effective as the behavior of oral melanoma differs from that of cutaneous

melanoma.[2,9] Immunotherapy with checkpoint inhibitors that allow T-cells to become activated against tumor cells has been successful in treating cutaneous melanoma in man, but less so for oral melanoma.[2] In dogs, the potential of identifying checkpoint inhibitors and developing immunotherapy is being explored.[9,11]

Contributing Institution:
NIH
9000 Rockville Pike
Building 28A, Room 117
Bethesda, MD 20892

JPC Diagnosis:
Oral cavity: Melanoma.
Oral mucosa: Stomatitis, ulcerative, focally extensive, marked with numerous yeast, pseudohyphae, hyphae, and cocci.

JPC Comment:
We repeated the same list of IHC and special stains outlined by the contributor and got nearly identical results. In particular, neoplastic cells were strongly and diffusely immunoreactive for PNL2, Melan-A Red, and SOX10, though they did not react with HMB-45 which may reflect a difference in lab assay performance. With our Fontana-Masson stain applied, approximately 5-10% of neoplastic cells have intracytoplasmic black granules (melanin) which is also evident on H&E to a lesser extent (figure 4-4). Conference participants felt that these results were consistent with the diagnosis of a melanoma but felt that there were enough granules evident on H&E alone to forgo the 'amelanotic' label. The exact cutline for having little melanin present may vary per pathologist and many hypopigmented lesions probably fall into the amelanotic camp. At the JPC, we typically withhold the qualifier of 'amelanotic' for cases that have no discernable melanin on H&E. To our knowledge, published reports of oral melanoma in the non-human primate remain rare in line with what the contributor notes.

The inclusion of electron microscopy in this case workup is a welcome addition (figure 4-5). Recognizing melanosomes on EM is helpful as they characteristically have an oblong shape that Dr. Bruce Williams swears looks like a watermelon (or perhaps a football) in second of the four phases of melanin synthesis that contributor highlights.

In addition, conference participants honed in on a second aspect of this case that the contributor may have curtailed given the lengthy write up on melanoma they provided. In the bottom left (approximately 8 o'clock on figure 4-2), the oral mucosa is ulcerated, edematous, and has several small blood vessels with clear indications of vasculitis. Immediately adjacent, there are numerous fungal mats that contain yeast, pseudohyphae, and hyphae as well as colonies of cocci. Participants felt that these changes were consistent with ulcerative stomatitis secondary to *Candida*. In the history provided for this case, there was no mention of immunosuppression (i.e. SHIV infection) or antibiotic use though both of these are reasonable differentials for this lesion alone. After careful discussion, we added a second morphologic diagnosis for this case (a rarity for neoplasms) as we felt that this process was not directly connected to the melanoma in this case given the lack of junctional activity and condition of the remaining portion of the oral mucosa. Lastly, tissue ID for this case was aided by the presence of plant material (food) in section, though other similar tissues with stratified epithelium in a primate include the vagina and sex skin.

References:

1. Albert DM, Dubielzig RR, Li Y, et al. Choroidal Melanoma Occurring in a Non-human Primate. *Arch Ophthalmol*. 2009;127(8):1080–1082.
2. Dika E, Lambertini M, Pellegrini C, et al.. Cutaneous and Mucosal Melanomas of Uncommon Sites: Where Do We Stand Now? *J Clin Med*. 2021 Jan 28;10(3):478.
3. D'Mello SA, Finlay GJ, Baguley BC, Askarian-Amiri ME. Signaling Pathways in Melanogenesis. *Int J Mol Sci*. 2016 Jul 15;17(7):1144.
4. Kambale Syaluha E, Zimmerman D, Ramer J, et al. Metastatic perioral melanoma in a wild mountain gorilla (Gorilla beringei beringei). *J Med Primatol*. 2021 Jun;50(3):197-200.
5. Lambert MW, Maddukuri S, Karanfilian KM, Elias ML, Lambert WC. The physiology of melanin deposition in health and disease. *Clin Dermatol*. 2019 Sep-Oct;37(5):402-417.
6. Mauldin EA, Peters-Kennedy J. Integumentary System. In: Maxie MG, ed. *Jubb, Kennedy & Palmer's Pathology of Domestic Animals*. Vol 1. 6th ed. St. Louis, MO: Elsevier; 2016:720-722.
7. Ordóñez, NG. Value of melanocytic-associated immunohistochemical markers in the diagnosis of malignant melanoma: a review and update. *Hum Pathol*. 2014 Feb;45(2):191-205.
8. Pellegrini G, Bienvenu JG, Meehan JT, et al. Cutaneous melanoma with metastasis in a cynomolgus monkey (Macaca fascicularis). *J Med Primatol*. 2009 Dec;38(6):444-7.
9. Prouteau A, André C. Canine Melanomas as Models for Human Melanomas: Clinical, Histological, and Genetic Comparison. *Genes (Basel)*. 2019 Jun 30;10(7):501.
10. Smedley RC, Lamoureux J, Sledge DG, Kiupel M. Immunohistochemical diagnosis of canine oral amelanotic melanocytic neoplasms. *Vet Pathol.* 2011 Jan;48(1):32-40.
11. Stevenson VB, Perry SN, Todd M, Huckle WR, LeRoith T. PD-1, PD-L1, and PD-L2 Gene Expression and Tumor Infiltrating Lymphocytes in Canine Melanoma. *Vet Pathol*. 2021 Jul;58(4):692-698.
12. Thomas NE, Kricker A, Waxweiler WT, et al. Comparison of Clinicopathologic Features and Survival of Histopathologically Amelanotic and Pigmented Melanomas: A Population-Based Study. *JAMA Dermatol*. 2014;150(12):1306–1314.
13. Van der Weyden L, Brenn T, Patton EE, Wood GA, Adams DJ. Spontaneously occurring melanoma in animals and their relevance to human melanoma. *J Pathol*. 2020;252(1):4-21.
14. Zerfas PM, Brinster LR, Starost MF, Burkholder TH, Raffeld M, Eckhaus MA. Amelanotic melanoma in a New Zealand White Rabbit (Oryctolagus cuniculus). *Vet Pathol*. 2010 Sep;47(5):977-81.